UC Berkeley

UC Berkeley Previously Published Works

Title

Fast-Response Operando Mass Spectrometry Demystifies C_2 Product Formation in Cu-Catalyzed CO and CO_2 Reduction: Burst of Ethylene Isotopologues

Permalink

https://escholarship.org/uc/item/89h9c1m9

Authors

Zeng, Helen J
Kim, Yesol
Yano, Junko
et al.

Publication Date

2026-09-08

DOI

10.26434/chemrxiv.15008486/v1

Copyright Information

This work is made available under the terms of a Creative Commons Attribution-NonCommercial-NoDerivatives License, available at https://creativecommons.org/licenses/by-nc-nd/4.0/

eScholarship.org Powered by the California Digital Library
University of California

8 September 2026

Fast-Response Operando Mass Spectrometry Demystifies C_2 Product Formation in Cu-Catalyzed CO and CO_2 Reduction: Burst of Ethylene Isotopologues

Helen J. Zeng[1], Yesol Kim[1], Junko Yano[2], Joel W. Ager[1,3,4]

1. Chemical Sciences Division, Lawrence Berkeley National Laboratory
2. Molecular Biophysics and Integrated Bioimaging Division, Lawrence Berkeley National Laboratory
3. Materials Sciences Division, Lawrence Berkeley National Laboratory
4. Department of Materials Science and Engineering, University of California, Berkeley

Abstract

It has been a long-standing challenge in electrocatalysis to measure product formation with kinetically relevant time resolution. Here, we couple a real-time gas analyzer mass spectrometer with a modified sampling inlet to a gas diffusion electrode cell, achieving sub-second time resolution for both reactant consumption and product formation. We focus on CO_2/CO reduction on oxide-derived Cu, motivated by the continuing interest in its reaction mechanism and its high selectivity to ethylene (C_2H_4) formation. Potential step experiments for CO reduction reveal that the initial consumption of CO is fast (< 1 s), but the appearance of C_2H_4 products can be 10 times slower, which we attribute to the time required for CO storage on the Cu surface and subsequent reconstruction into the active, C_{2+}-forming, configuration. Previous studies have reported that the co-feed of $^{12}CO_2$/^{13}CO results in the enhancement of ^{13}C-containing ethylene isotopologues, but the mechanism causing this remains unknown. Isotopic-labeled gas switching ($^{12}CO_2$-^{13}CO) experiments yield compelling evidence that ^{13}C species continue to exist for more than a minute at near proximity to or on the catalyst, even after the supply source has been cut off, evidenced by the significant enhancement of ^{13}C-containing ethylene isotopologues: pure ($^{13}C_2H_4$) and mixed ($^{13}C^{12}CH_4$), formed through a CO_2(g)-*CO pathway. Importantly, the size of the C_1 reservoir, the amount of $^{13}C^{12}CH_4$ made when CO_2 reacts with it, and the amount of Cu^+ that is removed are all in the micromole range. Thus,

Posted on 8 September 2026 — CC-BY-NC-ND 4.0 — This is a preprint and has not been peer reviewed. Data may be preliminary. —
https://doi.org/10.26434/chemrxiv.15008486/v1

the picture emerges that a monolayer is stripped off from the copper catalyst surface during the CO-CO_2 switch. Tracking of dynamic Cu surface insights (i.e., activation, dissolution and deactivation) provides valuable mechanistic insights for optimizing reaction conditions.

Posted on 8 September 2026 — CC-BY-NC-ND 4.0 — This is a preprint and has not been peer reviewed. Data may be preliminary. — https://doi.org/10.26434/chemrxiv.15008486/v1

Fast-Response Operando Mass Spectrometry Demystifies C_2 Product Formation in Cu-Catalyzed CO and CO_2 Reduction: Burst of Ethylene Isotopologues

Helen J. Zeng,[a] Yesol Kim,[a] Junko Yano[b,*] and Joel W. Ager[a,c,d,*]

[a] *Chemical Sciences Division, Lawrence Berkeley National Laboratory, Berkeley, CA 94720, USA*

[b] *Molecular Biophysics and Integrated Bioimaging Division, Lawrence Berkeley National Laboratory, Berkeley, CA 94720, USA*

[c] *Materials Sciences Division, Lawrence Berkeley National Laboratory, Berkeley, CA 94720, USA*

[d] *Department of Materials Science and Engineering, University of California, Berkeley, Berkeley, CA 94720, USA*

* Corresponding authors: jyano@lbl.gov, jwager@lbl.gov

Abstract

It has been a long-standing challenge in electrocatalysis to measure product formation with kinetically relevant time resolution. Here, we couple a real-time gas analyzer mass spectrometer with a modified sampling inlet to a gas diffusion electrode cell, achieving sub-second time resolution for both reactant consumption and product formation. We focus on CO_2/CO reduction on oxide-derived Cu, motivated by the continuing interest in its reaction mechanism and its high selectivity to ethylene (C_2H_4) formation. Potential step experiments for CO reduction reveal that the initial consumption of CO is fast (< 1 s), but the appearance of C_2H_4 products can be 10 times slower, which we attribute to the time required for CO storage on the Cu surface and subsequent reconstruction into the active, C_{2+}-forming, configuration. Previous studies have reported that the co-feed of $^{12}CO_2/^{13}CO$ results in the enhancement of ^{13}C-containing ethylene isotopologues, but the mechanism causing this remains unknown. Isotopic-labeled gas switching ($^{12}CO_2$-^{13}CO) experiments yield compelling evidence that ^{13}C species continue to exist for more than a minute at *near proximity to or on* the catalyst, even after the supply source has been cut off, evidenced by the significant enhancement of ^{13}C-containing ethylene isotopologues: pure ($^{13}C_2H_4$) and mixed ($^{13}C^{12}CH_4$), formed through a CO_2(g)-*CO pathway. Importantly, the size of the C_1 reservoir, the amount of $^{13}C^{12}CH_4$ made when CO_2 reacts with it, and the amount of Cu^+ that is removed are all in the micromole range. Thus, the picture emerges that a monolayer is stripped off from the copper catalyst surface during the CO-CO_2 switch. Tracking of dynamic Cu surface insights (i.e., activation, dissolution and deactivation) provides valuable mechanistic insights for optimizing reaction conditions.

Keywords: CO_2 reduction · electrochemistry · analytical chemistry · mass spectrometry · time-resolved product analysis

TOC Graphic

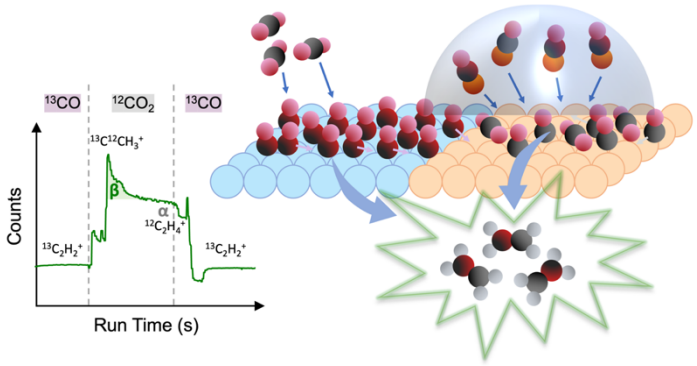
^{13}CO
$^{12}CO_2$
^{13}CO
$^{13}C^{12}CH_3^+$
β
α
$^{12}C_2H_4^+$
$^{13}C_2H_2^+$
$^{13}C_2H_2^+$
Counts
Run Time (s)

Introduction

Electrocatalysis features prominently in future concepts of chemical refineries which could be less reliant on fossil fuel inputs.[1,2] In this context, electrochemical CO_2 reduction (EC-CO_2R), and the related CO reduction (EC-COR) reaction, play a central role, as they can produce platform chemicals and fuels such as ethylene, methanol, and ethanol.[3–5] However, it has not yet been possible to achieve the combination of selectivity and lifetime in EC-CO_2R and EC-COR processes which would allow them to compete with the heterogenous catalysis approaches now used in the petrochemical industry.[6]

EC-CO_2R and EC-COR on Cu, which can yield multiple C_1 and C_{2+} products, has been an especially challenging case.[7,8] We note that most experimental studies in this area continue to operate in the steady-state domain, optimizing catalyst, cell design, operation and reaction conditions using classic, intermittent/batch analysis methods such as gas chromatography (GC), nuclear magnetic resonance (NMR), and/or high-performance liquid chromatography (HPLC) for product analysis.[9–11] At the same time, there is mounting experimental evidence that the EC-CO_2R/COR environment is highly dynamic with reaction intermediates such as *CO mediating surface restructuring.[12–14] Clearly, analytical techniques which can resolve these dynamic effects would be highly valuable.

Methods such as chemical transient kinetics (CTK), temporal analysis of products (TAP), steady state isotopic transient kinetic analysis (SSITKA) have been widely used for kinetic studies of thermal heterogenous catalysis.[15–21] However, there are key differences between thermal catalysis and electrocatalysis which prevent the direct adaptation of the former's techniques. First, in thermal catalysis, modulations in reaction rates induced by temperature changes are relatively slow, whereas in electrocatalysis reaction rates can be changed very quickly, and by orders of magnitude, via changes in the electrode potential. Secondly, in EC-CO_2R/COR electrocatalysis, all three phases of matter (gas, liquid, solid) are present in addition to the electrical potential, which rules out adapting surface science approaches, such as temperature programmed desorption. Finally, in the two-compartment H-cells which are used in many studies, gas phase products will accumulate in the headspace where their interdiffusion will smear out transient effects.

Differential electrochemical mass spectrometry (DEMS) addresses some of these challenges.[22] In a typical implementation, a modified H-cell geometry is used to allow sampling in the near vicinity of the working electrode. For example, a porous tip allows sampling of both gaseous and liquid products.[23–25] Due to the use of mass spectrometry, detection limits can be very good. In terms of partial current densities, these values are typically in the range of nanoamperes per square centimeter ($nA \cdot cm^{-2}$). However, there are limitations as well. Typical response to an abrupt input (e.g. a potential step) is ca. 10 seconds,[26] and overlapping fragmentation patterns from the typically employed electron impact (EI) ionization arise due to mass degenerate species from both gaseous and liquid products.[25] In 2019, Mayrhofer and co-workers developed the Electrochemical Time-Resolved Mass Spectrometry (EC-TRMS) method using electron ionization quadrupole mass spectrometer (EI-QMS) for gas products and direct analysis in real time time-of-flight mass spectrometer (DART-TOF-MS) for liquid products in a scanning flow cell with a response time of about 25 seconds.[27] The related membrane-introduction mass spectrometry (MIMS) method also has a slow response time (~tens of seconds to 1 min).[28,29]

Time resolution can be improved, in principle, via sampling from a gas diffusion electrode (GDE) cell; the gas transit time for a typical 1 cm^2 laboratory GDE is ca. 1 s.[30] Also, the higher current densities translate into higher concentrations of analytes: a 50 $mA \cdot cm^{-2}$ partial current density for ethylene in such a cell, which is easily achievable, translates to ca. 1% concentration at the exit, which is readily detected by MS. In 2022, Ager and co-workers further explored the potential of employing proton transfer reaction time-of-flight mass spectrometry (PTR-TOF-MS) in a GDE cell, achieving ppb-level detection limits with excellent mass resolution.[31] However, the temporal resolution was about 42 seconds.

Motivated by the need to improve time resolution, we developed a state-of-the-art, universal system (**Fig. 1a and Supplementary Fig. 1**) by coupling a real-time gas analyzer mass spectrometer (RTGA-MS) to a GDE cell to enable rapid and continuous monitoring of ppm-level products generated during an electrochemical CO_2 (or CO) reaction on a quantitative basis. Herein, by modification of the sampling inlet on the RTGA-MS, the response time of product gas sampling could be shortened down to as little as 1–3 s (vs. factory specification of 20 s, **Supplementary Figs. 2 and 3**). For the first time, a sharp rise in signal was detected to accomplish real-time tracking of changes on the sub-second time scale. Our current setup has been optimized to

efficiently transfer reaction products from the electrode surface in the GDE cell to the MS inlet, with the shortest time resolution reported thus far. It is able to detect both hydrogen and CO, and unaffected by water vapor in the effluent gas stream, deeming it more compatible for the GDE cell. In addition, consumption of reactants can also be followed in time, opening the possibility of measuring the dynamics of the carbon mass balance. Even though we employed EI, we show experiments in which the overlaps are manageable. Real-time insights into the chemical species formed at an electrode surface as the reaction progresses offer valuable temporal information for optimization of settings to achieve higher efficiency and selectivity, and to gain insights and understanding of the reaction mechanisms.

We employed our setup (**Fig. 1a and Supplementary Fig. 1**) on a class of 'oxide-derived' copper (OD-Cu) catalyst, prepared by oxidation and subsequent reduction, with the ability to boost C–C coupling (suppressing C_1 product) with a larger fraction of strong CO binding sites.[32,33] Having previously observed the depletion of a CO reservoir on OD-Cu, whereby COR reaction persists for up to 5 s after reactant supply had been curbed,[30] we now focus on its formation and its role in the chemical reaction network of COR/CO_2R. Improvements to RTGA-MS now allow sampling from 1 atm streams with < 1 s time resolution, defined as $t_{1/2}$ for step changes in concentration in the stream. The dynamic range of the method also allows for a close to complete carbon mass balance (excluding carbon species that dissolved in the electrolyte). We will elucidate the kinetics of reservoir formation and also show that it likely consists of hydrogenated C_1 species and the dissolution/redeposition of Cu^+ is also involved. The C_1 reservoir, once formed, becomes surprisingly reactive with CO_2, with transient rates of C_2H_4 production being nearly two times that of steady-state condition. Furthermore, we will discuss implications of the work in the context of some other recent studies.

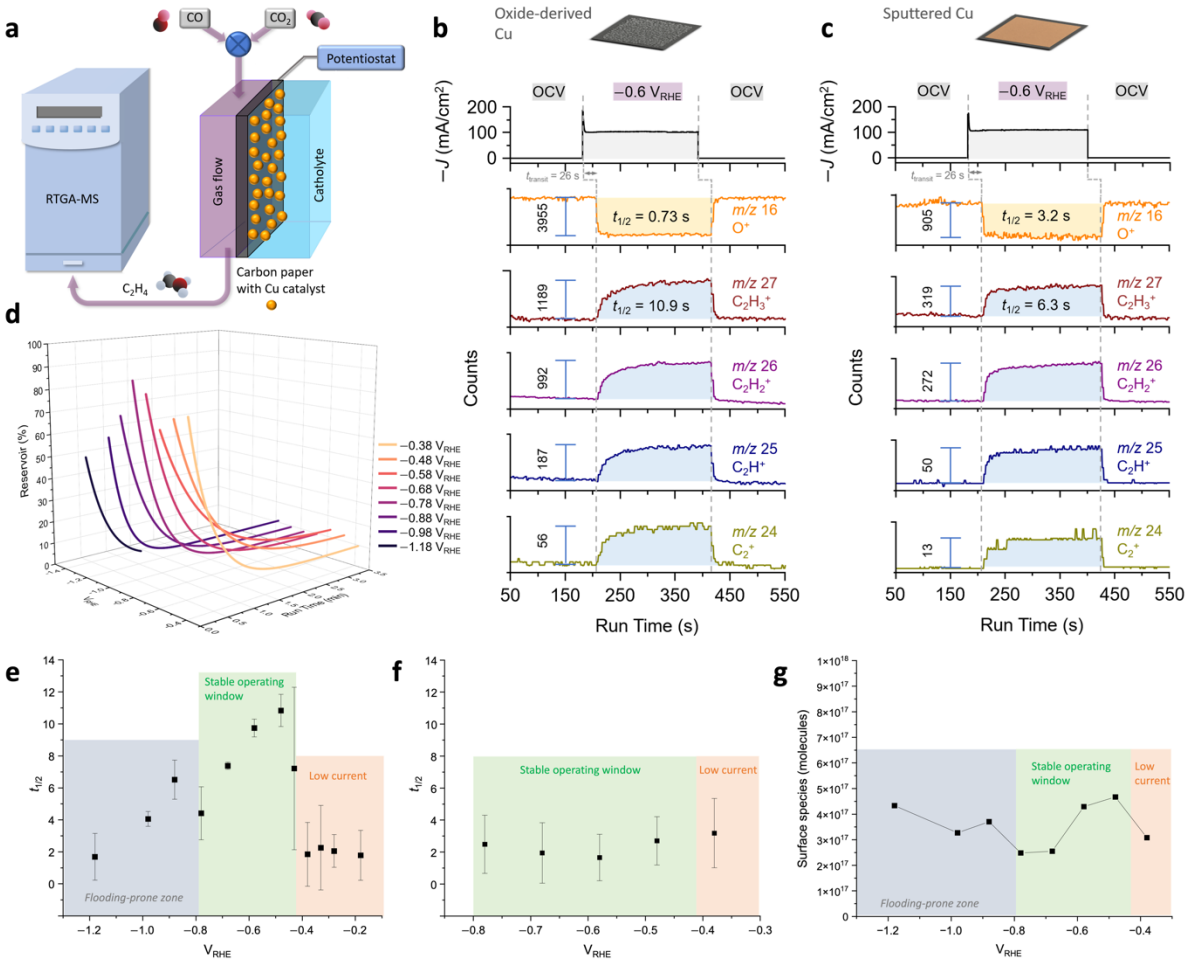

Fig. 1 | Operando mass spectrometric setup for tracking gas products and reactants from electrocatalysis (focusing on CORR) with sub-second time resolution. a, Operating electrocatalysts in a GDE geometry allows for rapid control of product feed via gas switching. The ideal approach to track sudden changes (e.g. gas switching, application of potential step, etc.) is to interface the GDE cell with high-sensitivity MS. Details of the entire setup can be found in **Supplementary Fig. 1**. **b,** The real-time plots of oxygen atom (O^+, *m/z* 16) corresponding to consumption of CO reactant, and the production of ethylene (C_2H_4), represented by its four fragment ions, evolved from CORR of OD-Cu NPs catalyst [−0.6 V_{RHE}, 1 M KOH, 5 standard cubic centimeters per minute (sccm) $^{12}CO(g)$]. The top panel shows the current density plot of the ^{12}CORR. After being held at open circuit voltage (OCV) for the first 3 min, a potential (–0.6 V_{RHE}) was applied and was held for 3.5 min, before it was switched off and returned to OCV. Note that there was a 26 seconds delay for the rise in the signal, due to time taken for the output gas stream to pass through the tubing connecting the GDE cell to the MS. **c,** Results obtained from sputtered Cu under the same experimental condition as **(b)**, with lowered yield. **d,** Potential-dependent, net flux of carbon going into the reservoir (%) over time from CORR of OD-Cu, reaching steady state after some time (> 1 min) once saturated. The first points of the curves are recorded after 6 s. Refer to **Supplementary Fig. 11** for detailed explanations. **e, f,** The $t_{1/2}$ values for **(e)** ethylene via the rising edge of *m/z* 27, and **(f)** CO by the initial falling edge

of *m/z* 16, obtained at different applied potentials, for the CORR of OD-Cu. **g,** Estimated CO/protonated C_1 species in reservoir at varied applied potentials.

Results and Discussion

Tracking ethylene evolution with OD-Cu during COR

To conduct a kinetic, carbon mass-balance experiment, we first prepared the GDE cell with the OD-Cu NP catalyst, following a protocol from our group.[30] We proceeded to study ^{12}CORR by applying a potential step (–0.6 V_{RHE}) to record its current density and observe the complex, kinetic behavior at the catalyst.[30] Concurrently, we measured the output gas stream with the RTGA-MS by tracking on the fragment ions of $^{12}C_2H_4$, with the real-time traces presented in **Fig. 1b**. These unique masses can be tracked with high fidelity, and do not overlap with fragments by other common gas species, either from atmosphere air or the gas product stream.[34] Compared with the ion fragments measured from pure C_2H_4 gas (**Supplementary Figs. 4–7 and Supplementary Table 1**), the recorded counts are tabulated in **Supplementary Table 2**, with their relative intensity ratio in good agreement. Due to the length of tubing (~1 m) connecting the GDE cell to the MS, there was a known transit time of 26 seconds (see **Methods**).[35]

In response to a potential step applied on the OD-Cu, the uptake of CO (O^+, *m/z* 16) occurs within sub-second ($t_{1/2}$ = 0.73 s) at 3.5th min mark. Strikingly, the appearance of ethylene product, represented by its four fragment ions with essentially the same time profile, is approximately 10× slower with a rounded rising edge. Interestingly, as we observe both CO and C_2H_4, we can estimate its selectivity in steady state: about 58.7% of the CO goes into C_2H_4 **(SI page S-15)**. However, it requires some time to approach steady state; appearance of C_2H_4 is delayed compared to CO consumption. The discrepancy during this time means that there must be a buildup of carbon species somewhere in the system, as more carbon atoms are entering rather than exiting.

Note that the *m/z* 16 trace was used, instead of *m/z* 28, for direct evidence of ^{12}CO (**Supplementary Fig. 8**), as the latter is dominated by the N_2 background in the mass spectrometer and also coincides with $^{12}C_2H_4^+$. Although this is a minor fragment (1.7%), as CO is difficult to ionize with EI, it is an advantage because the detector is unsaturated. The likelihood of methane appearing at *m/z* 16 has been eliminated, as this catalyst does not display any significant methane formation using a

GC previously.[30] To check this, we also turned to another indicator of methane (CH_3^+, *m/z* 15). Indeed, the absence of potential-induced changes in the trace of *m/z* 15 (**Supplementary Fig. 8**) confirms that this C_2H_4 formation on OD-Cu goes through the route via *CO intermediates.

Hydrogen is another possible gas product that should be considered. To investigate hydrogen evolution reaction (HER), a separate experiment under the same experimental conditions was conducted using another mass spectrometer (Pfeiffer OmniStar GSD 301-O1) that is capable of detecting low *m/z*, specifically hydrogen (**Supplementary Fig. 9**). The profile shape of the *m/z* 2 (H_2^+) shows a slightly shorter $t_{1/2}$. The appearance of hydrogen before C_2H_4 formation can account for some of the current that flows in the first 10 seconds as the reservoir is still forming, and will be discussed later in the context of proton-coupled electron transfer (PCET).

Observing CO reservoir formation and its behavior

The results obtained from OD-Cu NPs were also benchmarked against sputtered Cu, one of the most common thin-film preparation methods, but previously produced less ethylene via GC measurements under the same conditions.[30] As expected, the yield of ethylene has decreased by a factor of four, even at a similar current density. Notably, the shape profiles of the real-time traces (**Fig. 1c**) show a slower CO depletion and faster initial C_2H_4 production. As such, this highly sensitive technique is capable of revealing sample-dependent surface dynamics to distinguish performances.

To further investigate the appearance kinetics of C_2H_4, a survey of various applied voltages was conducted (with representative traces of $C_2H_3^+$, *m/z* 27, displayed in **Supplementary Fig. 10**). Interestingly, the $t_{1/2}$ values at very low applied potentials appear to be quite short and abrupt (**Fig. 1e**), which can be rationalized as the characteristic time of the C_2H_4-producing sites in the absence of reservoir, whereby barely any ethylene was produced. Eventually, a clear turning point appeared at −0.43 V_{RHE} and a maximum $t_{1/2}$ value was obtained at −0.48 V_{RHE}, that signals the onset and optimized potentials for reservoir formation, respectively. At low overpotential, we might be seeing intrinsic activity of active site, that is, they might be limited by C_1 reactant supply. As this depends critically on details of surface, we would expect scattered data points, which is indeed the case. As higher overpotentials were applied, the $t_{1/2}$ values gradually shortened, showing that the reservoir formation is potential-dependent. This is consistent with our previous findings, whereby

a delay time of 4–6 s was noted after gas feed was switched from CO to Ar (inert gas), depending on the cathode potential (i.e., longer delay time was noted at lower potential).[30] However, there are several notable differences between these studies. For example, the previous study relied on a mass flow meter, which was unable to detect small changes occurring in the region of less than −0.50 V_{RHE}. With the high-sensitivity mass spectrometer, we are now able to interrogate the lower extreme of the potential regions. In addition, the previous study was conducted at steady-state regions, whereas we hereby focus on the transformations at the start-up phase, and posited that the rising time provides direct insights into the initial and slower loading process of CO molecules on Cu (**Supplementary Fig. 11**).

Using calibration gases containing ppm-level ethylene (**Supplementary Fig. 7** and **Supplementary Tables 3 and 4**), the concentrations of ethylene produced with other isotopic gases (COR and CO_2R) are tabulated in **Supplementary Table 5**, and results in **Supplementary Figs. 12-15**. ^{13}CO is often employed in studies aimed at differentiating COR from $^{12}CO_2R$. For the same amount of input gas (5 sccm), ethylene obtained for CO_2RR is about halved compared to COR. Based on this, it can be inferred that the CO_2-to-CO reaction is more dominant, and that the CO-to-ethylene conversion is less likely to occur. Data obtained from the electrochemical runs, specific details and their related calculations are presented in the Supplementary Information (**Supplementary Figs. 16–27** and **Supplementary Tables 6–10**).

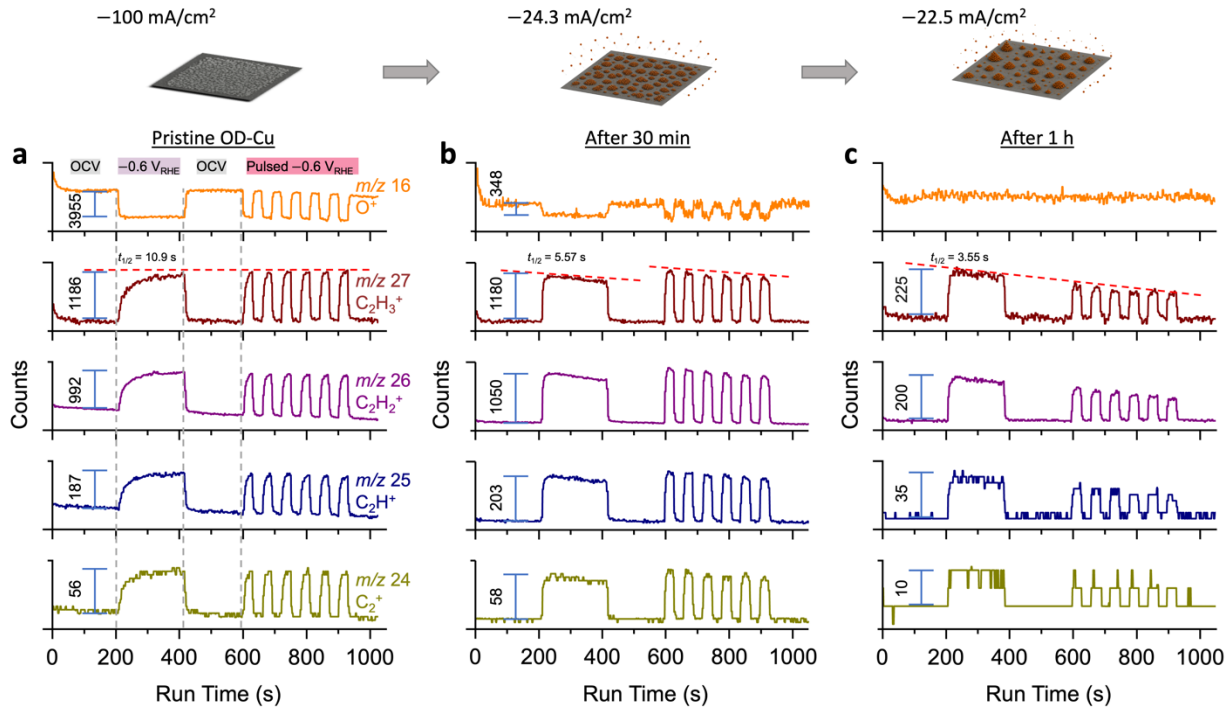

Fig. 2 | Real-time mass spectrometry tracks time-dependent morphological changes of catalyst, such as dissolution and degradation processes. a–c, Major catalytic events (activation, dissolution, and degradation) in CO reduction reaction captured by mass spectrometry in real-time. Real-time plots of masses corresponding to the four key fragment ions of ethylene formed under ^{12}CORR of **(a)** a pristine OD-Cu sample (5 sccm CO), **(b)** OD-Cu after 30 min of use (7 sccm CO), and **(c)** OD-Cu after more than 1 h of use (10 sccm CO). The first 550 s of **(a)** is also displayed in Fig. 1b. The long (3.5 min) and short (30 s) voltage pulses that were applied at –0.6 V_{RHE} triggered the rise of signals from OCV status. The flow rate of gas was increased to expedite and amplify the degradation event.

Monitoring Cu activation/deactivation, dissolution and degradation

Morphological changes on the catalytic surface has been a topic of interest and the ability to track them under operando conditions has been sought-after.[36] Depending on the reaction conditions and protocols applied, results can vary drastically with time. **Figs. 2a–c** presents the ethylene fragment ion signals that were obtained during ^{12}COR of OD-Cu sample that is pristine (**Fig. 2a**), after 30 min (**Fig. 2b**), and 1 h of use (**Fig. 2c**). The first longer pulses (3.5 min) in **Fig. 2a** is the same as that in **Fig. 1b**. Following this, a series of short pulses (30 s) was applied. This pulsing scheme was performed to demonstrate the fast time response of the instrument and test the notion that reoxidation of Cu by continuous oxidation/reduction cycles helps to regenerate catalytic

activity.[12,37,38] Pulsing was recognized as one of the most effective strategies to address long-standing instability problems.[39]

For the fresh OD-Cu sample, the signal for the product shows a curved rising edge, which gradually reaches steadiness (red dashed line in **Fig. 2a**). The short pulses also continue to show curved rising edges as the catalyst is still undergoing activation, but reach steady state faster than the first pulse. By the second use (**Fig. 2b**), $t_{1/2}$ decreases to 5.57 s after OCV, indicating that there is no need to fill up the reservoir as much as before. At this point, the catalyst is still recoverable. However, the pulse signal drops immediately and continuously, even at constant applied voltage, which may be related to Cu dissolution.[40–42] It is evident that at the third run (**Fig. 2c**), $t_{1/2}$ became even shorter (3.55 s). The downward sloping trend continues even to the shorter pulses, marking a significant degradation of the catalyst that is unrecoverable. Current density goes down, and the lack of changes in the O^+ (*m/z* 16) trace suggests lowered CO uptake from the gas stream, due to catalyst deactivation. Hence, our tracking in real time indicate how changes in catalyst directly affects product generation. Reoxidation helps to maintain the quality of the catalyst to some extent, but its activity still greatly diminishes with extended use (**Supplementary Fig. 28**).[43–45]

Determining the size and species of the CO reservoir

By conducting an approximate calculation, we quantified the number of CO molecules in the reservoir (**SI page S-27**). The calculated value lies fairly close to that of the Cu atoms on the surface of the 25 nm OD-Cu NPs (mol/cm^2; 1 cm^2 electrode) that was previously determined by applying a roughness factor that was normalized to measurements conducted on flat Cu foil.[30] The corresponding electrochemical surface area (ECSA) calculations are presented in **SI page S-28**.

Crucially, the current density traces also reveal that the catalyst surface is taking up electrons in addition to CO. Based on the known PCET mechanism for creating C_1 and C_2 products on Cu (pathways in **Supplementary Fig. 29**), the H^+/e^- pairs that would be created in the initial phase is estimated to be 1-2 per CO molecule in the reservoir. Thus, a large fraction of the adsorbed CO molecules could be in the form of partially hydrogenated carbon species $*COH_x$, assuming that the electrons are going to the same place. As we note that repeated cycling degrades the catalyst (**Fig. 2**), it could be related to CO-mediated 'ejection' as reported by Yang et al.[14] As invoked very

recently, monovalent Cu cations can possibly detach from the surface in the form of Cu^+-CO species, a point to which we will return to below.[12] While these initial studies have shed light on the possibility of the Cu^+-CO species, this topic will be further explored in our following experiments.

Demystifying ethylene enhancement by isotope gas switching experiment

To investigate the reactivity of the CO reservoir, we conducted fast switching experiment of $^{12}CO_2$ and ^{13}CO input gases at constant potential. We aimed to deconvolute CO_2RR and CORR and identify their main mechanisms. As we hypothesize that there are reservoir sites on Cu to store CO molecules, with the advent of this instrument it is possible to detect the appearance of the mixed carbon ethylene ($^{13}C^{12}CH_4$) upon switching gases with different carbon isotopes. Based on past understanding, two major postulations were proposed: **(1)** $^{12}CO_2$ would first be reduced to ^{12}CO, due to the presence of active sites that favor this first reaction step, which are presumably stored, followed by incoming ^{13}CO which will react with the existing $*^{12}CO$ on the surface to become further reduced to $^{13}C^{12}CH_4$, or **(2)** ^{13}CO could be stored up and $*^{12}CO$ from $^{12}CO_2R$ would give rise to the C-C coupling.

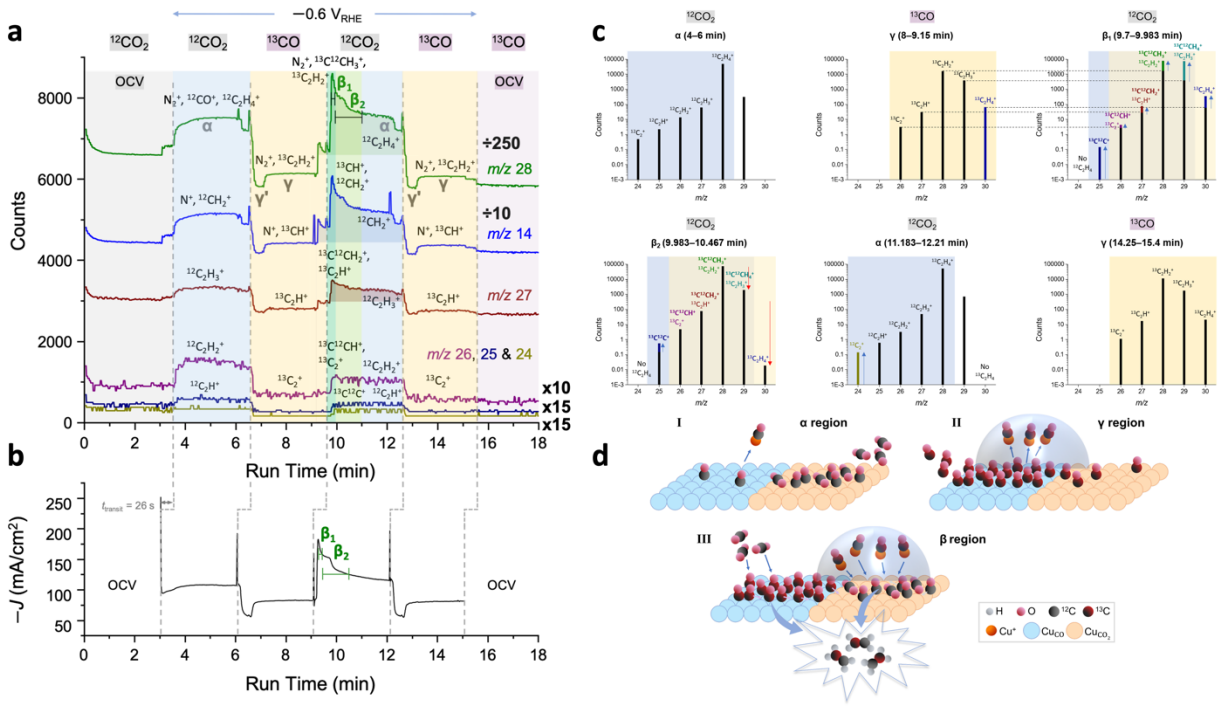

Fig. 3 | $^{12}CO_2$-^{13}CO gas switching experiment of OD-Cu catalyst (1 M KOH). a, Real-time plot of masses from switching between $^{12}CO_2$ and ^{13}CO gases (1:1, both gases set to 5 sccm), as indicated by the colored regions. From 3–15 min, a constant voltage potential (–0.6 V_{RHE}) was applied. A sudden spike in signal intensity was noted at 9.7 min for *m/z* 28 (alongside similarly shaped traces) with two sloped declines (labeled as β_1 and β_2), and eventually returned to steady-state (α phase of $^{12}CO_2RR$). **b,** The current density plot of the run also shows a sharply increased current density at the β_{1+2} regions, related to the electrons consumed to drive product formation. Thus, the spikes from the products directly correspond to spikes in current, and are not as a result of sudden release of preformed bubbles. **c,** Mass spectra (OCV-background subtracted) extracted from six different time periods in **(a)**. Counts are plotted to log scale, and colored bars indicate the most notable changes in masses. The resulting signals from product formation reveal that the switch from $^{12}CO_2$ to ^{13}CO forms a substantial amount of *m/z* 29 (teal) and *m/z* 30 (blue) in β_1, representing $^{13}C^{12}CH_4$ and $^{13}C_2H_4$ respectively. Note that N_2 and CO are present in these mass spectra. **d,** Illustrations depicting the mechanistic scenarios at each time frame. **(I)** $^{12}CO_2$ is first adsorbed and reduced to ^{12}CO on Cu_{CO_2}, which migrates to Cu_{CO}, and forms less ethylene. Cu^+-^{12}CO may also leave the surface, but this is a minor event due to less ^{12}CO produced. **(II)** More $*^{13}CO$ are stored on Cu_{CO}, followed by the C–C conversion to ethylene, resulting in more Cu^+-^{13}CO. **(III)** The presence of Cu^+-^{13}CO and $*^{13}CO$ lead to at least two β modes of $^{13}C^{12}CH_4$: **(i)** $^{12}CO_2$ directly reacting with $*^{13}CO$, **(ii)** C–C coupling between Cu^+-^{13}CO and freshly formed $*^{12}CO$, during which the deposition of Cu^+-^{13}CO is accelerated by $*^{12}COO^-$ and **(iii)** C–C coupling between $*^{13}CO$ residing on Cu_{CO} and $*^{12}CO$ that migrates over. Cu_{CO} could be related to kinks or defect sites and Cu_{CO_2} may be stable low-Miller indexed surfaces such as Cu(111).[46–48]

Initially, applying a potential step (–0.6 V_{RHE}) while flowing $^{12}CO_2$ yielded some ethylene by an increase of *m/z* 28 (green trace) at the 3.5th min, labeled as the α region (**Fig. 3a**). While the potential remained on, the gas was switched to ^{13}CO, whereby the *m/z* 28 signal then drops to the lowest level, then subsequently recovering in signal by a bit from some evolved $^{13}C_2H_2^+$. The origin of the small step changes in the first ~26 seconds after gas switching (right before the gray dashed lines), and the overview of changes in *m/z* 28 and 29 are provided in **Supplementary Fig. 30**. For detailed composition analyses, such as the average readout values over the time range, see **Supplementary Tables 11–18**. Another corresponding small bump can be seen for the profile of *m/z* 29 at the same time, which represents incoming ^{13}CO. These signals then reach steady-state operation (γ region, ^{13}COR), with $^{13}CO^+$ (unreacted) and evolved $^{13}C_2H_3^+$ (minority species). The gas feed was changed back to $^{12}CO_2$, resulting in the appearance of a prominent spike (labeled as β) in the *m/z* 28 signal, which may be a result of the evolution of $^{13}C_2H_2^+$ and $^{13}C^{12}CH_3^+$. A considerable amount of ^{12}CO had been consumed to create the spike. Then at 11.2th min for ~1 min, the signal flattens out (residual ^{13}CO supply had been fully diminished in **Supplementary Fig. 31**), resulting in solely ^{12}C products ($^{12}C_2H_4$) being formed. At the 12th min, $^{12}CO_2$ was then switched to the ^{13}CO once again (second γ region). There was a repeatable transient suppression of current when CO shows up to a CO_2-prepared surface (γ').

Surprisingly, based on our results, we postulate that the sharpest spike (β_1) may be indicative of a different type of Eley-Rideal (ER) mechanism,[49] whereby $^{12}CO_2$ gas molecules could directly react with the adsorbed $*^{13}CO$-prepared surface, forming the mixed $^{13}C^{12}C$ products. Prior to our current work, this mechanistic pathway had rarely been considered and had not been experimentally validated. By purposely creating a surface environment with a high coverage of C_1 intermediates and bombardment of $CO_2(g)$ by fast switching, this increase in signal could only arise from the ongoing reduction reaction, due to presence of stored ^{13}CO. The steepest drop occurs for the first 17 seconds (β_1), followed by a second decline (β_2) with a different slope, altogether lasting a total of 1.5 minutes. Corresponding to this, we see a large increase of the current density (**Fig. 3b**), higher than for CO_2R or COR in steady state, which indicates a vigorous reaction for the β_{1+2} phase formation, followed by a 'slow burn' to deplete all the stored CO. As the switch from $^{12}CO_2R$ to ^{13}COR did not result in a significant amount of mixed $^{13}C^{12}CH_4$ product, the other possible type of ER mechanism via *CO and CO(g) can be ruled out.[46] Without such high level of time

resolution, this effect may be ironed out and could have gone unnoticed, and so we are now able to resolve multiple reaction mechanisms at play in time.

The same 'trickling down' signal pattern was also reflected in *m/z* 14 ($^{13}CH^+$) and *m/z* 27 ($^{13}C^{12}CH_2^+$, $^{13}C_2H^+$) traces (in blue and maroon). On the other hand, the *m/z* 24–26 traces remain relatively flat, which are telltale signs that the *m/z* 27 and 28 traces represent some ^{13}C-containing species, as ^{13}C will not have major contributions to the masses 25 and below. A closer inspection of the *m/z* 26 trace revealed a tiny bump, possibly due to some $^{13}C_2^+$ and $^{13}C^{12}CH^+$. The traces *m/z* 12 and 16 relating to $^{12}C^+$ and O^+, and consequently, ^{12}CO, display the opposite trend of that (**Supplementary Fig. 32**).

To elucidate the CO_2-CO switching experiment more quantitatively, **Fig. 3c** presents a series of mass spectra averaged over different time periods from the real-time plots in **Fig. 3a**, which have been background-subtracted with their respective regions at OCV, and therefore represent products that had been electrochemically generated. The first panel shows the mass spectrum obtained for $^{12}CO_2RR$, and *m/z* 28 signal dominates due to presence of some N_2, but mostly from the ionization of $^{12}CO_2$, and some ^{12}CO and $^{12}C_2H_4$ products. As the gas was switched to ^{13}CO, formation of $^{13}C_2H_4$ (30 amu) led to increased *m/z* 29 and *m/z* 30 signals. Surprisingly, the switch from ^{13}CO to $^{12}CO_2$ resulted in a significant enhancement of *m/z* 25–30 signals, particularly *m/z* 28 and 29. The signals of *m/z* 27 doubled, *m/z* 28 quadrupled (1.6× compared to α region of $^{12}CO_2R$), *m/z* 29 by twenty-fold, and *m/z* 30 by five-fold, compared to the γ region (^{13}COR).

Interestingly, the complete absence of *m/z* 24 suggests that the $^{12}C_2H_4$ isotopologue was not electrochemically generated. The outburst of *m/z* 28–30 ions at β_1, can be assigned to the formation of mixed $^{13}C^{12}CH_4$ and pure $^{13}C_2H_4$ ethylene products. Interestingly, the ^{13}C-^{13}C formation rate is also increased, so CO_2 makes the coupling of the C_1 species in the reservoir faster. This is consistent with previous studies that had demonstrated that there are much higher levels of ^{13}C incorporation into the C_{2+} products than would be typically expected.[46,50,51] The *m/z* 29 and 30 signal then depleted substantially at the β_2 region, owing to the eventual consumption of ^{13}CO and displacement by the incoming ^{12}CO species. Detailed mass analysis reveals that the amount of pure $^{13}C_2H_4$ ethylene drastically reduces, while the mixed $^{13}C^{12}CH_4$ ethylene increases (**Supplementary Table 15**). The appearance of two falling edge slopes of β suggests that at least two different pathways could be at play.

Furthermore, we also conducted the $^{12}CO_2$-^{13}CO switching experiment at other potentials within the optimized region (−0.48 V_{RHE} and −0.78 V_{RHE}, **Supplementary Figs. 33–36**), reaffirming that the choice of in-depth study at −0.6 V_{RHE} condition is optimal as the β_{1+2} phase features are maximized, while maintaining relative stability. At higher potentials, the likelihood of GDE cell flooding increases and also, the production of liquid C_{2+} products start to dominate, resulting in significant overlapping of mass degenerate ions. Interestingly, at −0.78 V_{RHE}, a moderately-sized bump appeared about 1.5 min after the switch from $^{12}CO_2$ to ^{13}CO, for *m/z* 28, 27 and 14, with a corresponding dip in the *m/z* 30 trace, which suggests the complete depletion of $*^{12}CO$ as indicated by a quick outburst of ^{12}C-containing products. This provides clues that the $*^{12}CO$ generated from $^{12}CO_2RR$ in the earlier step is capable of remaining in the system for quite some time, even during $^{13}CORR$. The total duration of ~1.5 min is also consistent with that of the above β_{1+2} region as mentioned earlier. To check if these results were indeed influenced by the *CO storage ability of the catalyst, the switching experiment was performed with sputtered Cu sample, which indeed, yielded a blunt version of β_{1+2} (**Supplementary Fig. 37**).

A co-electrolysis experiment with a mixed gaseous ^{13}CO and $^{12}CO_2$ (70:30) stream was also performed to gain further insights into the distribution of ethylene isotopologues. This ratio was chosen as it had been previously determined that it would allow similar rates of $*^{13}CO$ and $*^{12}CO$ formation to occur in an H-cell, although we note that there may be some differences with the GDE cell.[45] The current density ($J = \sim -80$ mA/cm^2) is similar to, but slightly lower than $^{12}CO_2R$. System reaches steady state more quickly, in 5 seconds. Indeed, a high fraction of ^{13}C in ethylene was confirmed as shown in **Fig. 4a** with a ^{12}C:^{13}C ratio of about 1:4 (**Supplementary Tables 19 and 20**). Similar to the switching experiment, no $^{12}C_2H_4$ isotopologue was observed, because based on **Fig. 1b** ($^{12}CO_2R$), there would have been a readout at *m/z* 24 if there was any $^{12}C_2H_4$. Enhancements for the same *m/z* values (*m/z* 25–30) were similarly noted as the $^{12}CO_2$-^{13}CO switching experiment (**Fig. 3a**), thus supporting the previous mass assignments at various time points regarding the formation of $^{13}C_2H_4$ and $^{13}C^{12}CH_4$.

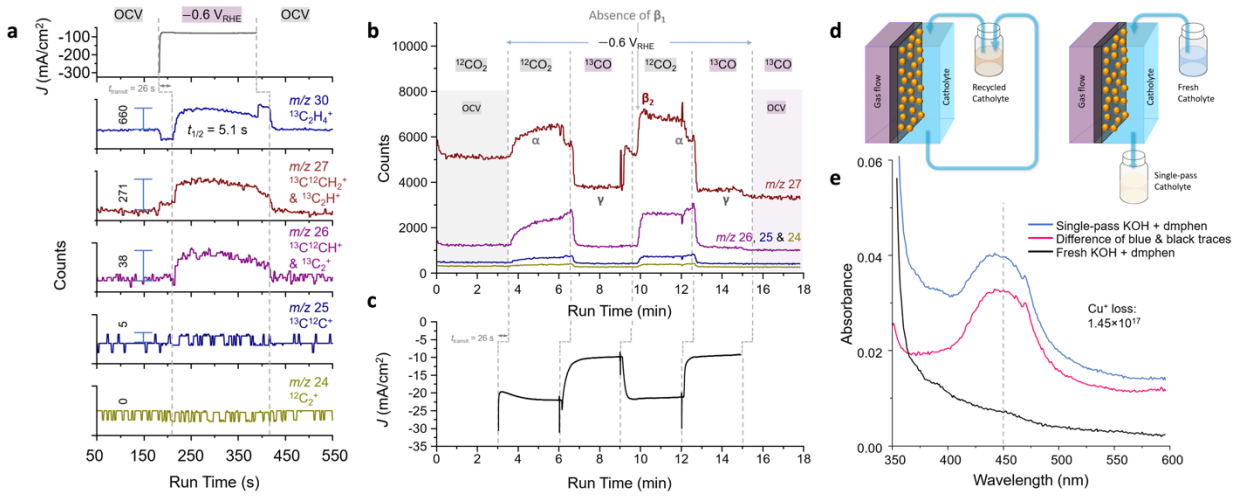

Fig. 4 | Additional experiments of using mixed isotope gases to generate mixed isotopologue ethylene product and fresh electrolyte to remove dissoluted Cu species. a, Real-time mass spectrometric traces of the 70:30 $^{13}CO/^{12}CO_2$ co-feed [1.5 sccm $^{12}CO_2$(g) and 3.5 sccm ^{13}CO(g)] with the OD-Cu catalyst (−0.6 V_{RHE}, 1 M KOH). The absence of *m/z* 24 ($^{12}C_2^+$) signal directly proves that all of the ethylene formed contain ^{13}C, either as mixed ($^{13}C^{12}C$) or pure $^{13}C_2$ ethylene.[46,50,51] An enhancement of ethylene (47.8%) was noted (see Supplementary Information). The top panel shows the current density trace. **b,** Detection of Cu loss via fresh electrolyte (single-pass). Real-time plots of masses for $^{12}CO_2$-^{13}CO switching experiment at the same voltage (–0.6 V_{RHE}) to Fig. 3, with fresh electrolyte. From 3–15 min, a constant voltage potential was applied. A small spike in signal intensity was noted at ~10 min for *m/z* 27 (and other similarly shaped traces plotted here for comparison) with only one sloped decline (labeled as β_2) with an absence of β_1 (position marked in light gray), and eventually returning back to steady-state (α phase of $^{12}CO_2$RR). One part of the reservoir is being formed, while the other is not. **c,** The current density plot of the run also shows a much less pronounced bump in the β region. **d,** Schematic of the usual GDE setup (left) compared to this experiment (right). **e,** Detection of Cu species in electrolyte (1 M KOH) via ex-situ UV-Vis spectroscopy. The plot displays the difference spectra of fresh electrolyte with and without the ligand (black), used electrolyte with and without the ligand (blue), and fresh and used electrolytes both with added ligand (red). The measured absorption at 450 nm indicates the presence of $[Cu(dmphen)_2]^+$, meaning that Cu loss had occurred.

Investigating the origins of β_1 and β_2

This leads to the question as to what the highly reactive species driving the ethylene enhancement at β_2 could be. It is plausible that some of the origin of this *m/z* 29 species comes from the recovery of the Cu^+-CO complex species that lurk nearby.[12] This is also further supported by our direct observation of the Cu dissolution process (**Fig. 2b**). A likely reaction mechanism for this would be that a $^{12}CO_2$ molecule is first adsorbed on the Cu_{CO_2} site, to form a bent activated $*COO^-$ species.[52] The negatively-charged adsorbate would attract the Cu^+-^{13}CO complex to form the ethylene. This Langmiur–Hinshelwood (LH) pathway, together with the ER mechanism identified earlier, would account for the largest β_1 peak. As the signal for *m/z* 30 mostly disappeared upon the β_2 region (**Fig. 3c**), the source for the 3× enhancement of $^{13}C_2H_4$ at β_1 was likely also from the recovered Cu^+-^{13}CO molecules. Throughout the entire β, the C-C coupling (usual LH) between $*^{12}CO$ reduced from CO_2(g) on Cu(111) and $*^{13}CO$, as well as between two $*^{13}CO$, are also occurring, but these do not account for the enhancements.

Based on the $^{12}CO_2$-^{13}CO switching experiment, the ^{13}C fraction was identified to be 0.873 at the beginning, and drops to 0.581, with an average of 0.751 over the entire β region, meaning that ^{12}C:^{13}C was about 1:3 (**Supplementary Tables 15–18**). The absence of this β_1 event in the switching experiments of ^{13}CO and ^{12}CO gases (**Supplementary Figs. 38–40, Supplementary Table 21**) confirms that the *CO generated by CO and CO_2 gases exhibit remarkably different behavior in terms of storage capabilities and play separate roles. The $^{13}C^{12}CH_4$ mixed ethylene continues to be detected in the β_2 phase. Subsequently, the *m/z* 28 signal took an extended 1.5 min (β_{1+2} region) to recover back to the α state, suggesting that ^{13}C species continues to linger at close proximity to the catalyst, likely from slow migration of $*^{13}CO$ from reservoir storage sites on the catalytic surface, consistent with our previous report.[30]

As our experiments typically recycle a fixed volume of electrolyte (5 ml of 1 M KOH for the catholyte and anolyte, respectively), we also postulated that it may be possible to remove some of the dissolved Cu species at near-proximity to the OD-Cu, by conducting another experiment whereby the electrolyte is continuously refreshed (no cycling back in). Our hypothesis is that if the previous β feature is a result of this soluble intermediate, then the reduction of this species should diminish the appearance of β. **Fig. 4b** presents the scenario at −0.6 V_{RHE} condition with fresh electrolyte supply, whereby the β_2 still remains but β_1 has completely disappeared, which is

also absent in its current density trace (**Fig. 4c**). The catholyte that had exited the cell (**Fig. 4d**) was also subjected to a neocuproine (2,9-dimethyl-1,10-phenanthroline or dmphen) ligand test using UV-Vis spectroscopy, and the phenanthroline-bound Cu intermediate $[Cu(dmphen)_2]^+$ was optically detected at 450 nm (**Fig. 4e**). About 0.24 μmol of Cu^+ was lost during this run. Previously, detection of such complexes had been conducted in-situ,[12] but we show that it is possible to conduct such measurements ex-situ. The Cu dissolution process tracked under the different isotopic gases are presented in **Supplementary Fig. 41**, as reference. Results show that under single gases, copper ions are removed on the order of 10^{16}, which is one order less than for the switching experiment, confirming a synergetic effect of two gases. Validation of presence of Cu^+-CO in the electrolyte shows that these species have direct mechanistic implications on the formation of mixed ethylene isotopologues.

Resolving effects from reactants on the ethylene enhancement

There has been a huge interest regarding the exact roles of CO_2 and CO in the C_2 product formation (i.e., ethylene), with prior works experimentally addressing this by steady-state isotopic labeling studies. In 2018, Lum and Ager used a mixed gas of $^{13}CO/^{12}CO_2$ to show that OD-Cu catalysts can have three different types of active sites for C–C coupling (one that favors formation of ethanol and acetate, another that produces ethylene and the third which produces 1-propanol).[50] In the year following, Strasser and co-workers studied CuO_x nanoparticles in DEMS, and reported that this mixed $^{13}CO/^{12}CO_2$ co-feed resulted in an 50% enhancement in the production of C_2H_4.[53,54] More recently in 2023, Xu and co-workers used surface-enhanced infrared absorption spectroscopy (SEIRAS) and found that the presence of CO_2 had a pronounced beneficial effect on the CORR, by analysis of the isotopologue distributions of products, also using mixtures of $^{13}CO/^{12}CO_2$.[46,51] Although both groups proposed and relied on a two-site model (Cu_{CO} and Cu_{CO_2}) to address deviations from binomial distribution of ^{12}C vs. ^{13}C in ethylene, potentially arising from surface inhomogeneity, the consistently higher ^{13}C incorporation and promoting effect from CO_2 remain largely a mystery. Unlike prior studies that used mixed gas co-feed, we switched between the two different gases in order to track changes induced at short timescales to reveal the manifestation of stored CO, as well as the promoting effect from CO_2.

Very recently, a detailed theoretical study conducted by Cheng and co-workers employed DFT calculations (PBE-D3/def2-SVP level of theory) and a constant electrode potential model demonstrated that CO_2 + $*C_1$ couplings on Cu(100) surfaces is both kinetically favorable and thermodynamically preferred (**Supplementary Fig. 42**).[55] Seven of the nine potential $*C_1$ intermediates considered were found to favor CO_2 over *CO under alkaline conditions. Indeed, we provide compelling evidence of this happening at β_1. In-depth deconvolution of ^{13}C-containing ethylene produced in the β region, based on integration of areas under curves (**SI pages S-54 to S-57**), revealed that the number of ^{13}CO molecules required to generate the enhanced ethylene production during β_{1+2} is of a similar scale to the expected initial size of ^{13}CO reservoir (**Supplementary Fig. 43**). During β_1, the majority of ethylene are pure $^{13}C_2H_4$ via stored $*^{13}$CO, with 22% of total ethylene arising from the direct CO_2 + $*C_1$ pathway.[55]

In β_2, the mixed $^{13}C^{12}CH_4$ dominates, along with the continued recovery of Cu^+-^{13}CO to contribute to the overall ethylene enhancement effect. Despite having a completely filled $3d^{10}$ shell, Cu^+ binds strongly to CO via synergistic bonding; the CO molecule donates a lone pair from its carbon atom into the vacant 4*s*/4*p* orbitals of Cu^+, while the filled 3*d* orbitals of Cu^+ pump electron density back into the empty π* (anti-bonding) orbitals of CO. The mechanism regarding Cu^+-CO species proposed by Buonsanti and co-workers,[12] had been further revised by Zheng's team that this process likely involves an amorphous interphase (**Supplementary Fig. 44**), monitored through TEM.[56] Interestingly, the visual appearance of the amorphous interphase occurs within 0.6-0.8 s, which matches the time ($t_{1/2}$ = 0.73 s) at which CO was rapidly depleted in our mass spectrometric traces (**Fig. 1b**). As such, stored CO may have been quickly transported into this layer.

Therefore, our results and rigorous interpretations through a series of control experiments enables us to nicely tie all of the previous proposed mechanisms and existing models together (**Supplementary Fig. 45**) to describe an overall picture of CO reservoir formation on oxidized Cu and its effects on COR/CO_2R reactions, as well as unravel why and how co-electrolysis results in enhanced multicarbon product formation.

Conclusions

In conclusion, we have developed a new setup to closely monitor COR and CO_2R reaction progress of copper in GDE cell, by combining it with a real-time gas analyzer (RTGA) mass spectrometer instrument with fast time resolution (< 1 s). The GDE-RTGA-MS integrated system allows detailed, real-time, qualitative, and quantitative chemical analysis, progressing beyond routine sampling methods such as GC, GC-MS, mass flow meter or conventional EC-MS setups. For complex heterogeneous catalysts, work cannot be interpreted in a framework of single active sites. We have demonstrated that the RTGA-MS unveils and tracks key events that occur at different time points in the reaction, such as the catalyst activation, uptake of CO molecules from the gas stream to the catalyst surface, conversion to ethylene, catalyst dissolution and degradation.

Most importantly, this technique unlocks the unique ability to quantify the size of the CO reservoir stored on the Cu catalyst across a wide voltage range. By deliberately forming a CO reservoir and using CO_2 gas as a trigger for initiating the reaction, we obtained direct evidence with the RT-MS that COR continues for an extended time (~1.5 min), even after its supply had been curbed. This strongly supports the presence of CO storage sites, and the importance of considering surface Cu site heterogeneity.[30,57] Distinctions could be drawn between electrogenerated CO vs. CO as is, with enhanced ethylene formation from the latter. The synergistic effect of $^{12}CO_2$ and ^{13}CO was captured, attributed to the complex interplay of recovery of dissoluted Cu^+-CO species, storage and migration mechanisms of CO, together with the promoting effect of CO_2 via the Eley-Rideal mechanism, pushing the reaction toward the 'CO_2(g)-*CO pathway' uncovered with this work. Our findings manage to support and reconciliate many of the interpretations drawn in earlier works by providing further insights.

As we herald a new era of operando research, we envision that this new tool will provide exciting opportunities to study various catalysts in GDE systems under different conditions.[58] With the ability to resolve processes that occur at short timescales, it unlocks new capabilities to study catalysts and their microscopic environments in greater detail, under practical electrochemical laboratory settings. Improving our fundamental understanding of such systems is a prerequisite in order to expedite the development toward rational design of new, robust catalysts and stability improvements for selective electrosynthesis under dynamic operation. Since the RTGAs has been used in many other areas of research (e.g. petrochemical, syngas, biofuels, toxic gas detection,

etc.), we expect that this improvement made to enable faster gas sampling may also have wider applications beyond GDE-based flow cells.

Methods

Materials

All chemical reagents were used as purchased without further purification. As-purchased active materials include 25 nm TEM Cu nanoparticles (Sigma-Aldrich). Catalyst ink dispersions were created using isopropanol (≥ 99.5%, Sigma-Aldrich), with Nafion (Ion Power, Chemours D521) as the ionomer. The catalysts were supported on 315 μm carbon paper (Sigracet 39BB, Fuel Cell Store). The electrolyte used is potassium hydroxide (85%, Fisher Scientific). ^{12}CO (99.999%) gas cylinder was purchased from Airgas. $^{12}CO_2$ (99.999%) gas cylinder was purchased from Praxair. $^{12}C_2H_4$ (99.5+%), ^{13}CO (99%), and $^{13}CO_2$ (99%) gas lecture bottles were purchased from Sigma-Aldrich. Neocuproine (≥ 98%) was purchased from Sigma-Aldrich.

Synthesis of Catalysts and Preparation of Gas Diffusion Electrodes

Preparation of OD-Cu NPs and gas diffusion electrodes (GDE) were prepared following previously published protocols.[30]

OD-Cu NPs

In brief, OD-Cu NPs was prepared by heating Cu NPs in a tube furnace at 500°C, open to air. The ramping speed was 5°C/min, the temperature was held for 1 hour, and ramp-down time was 5 minutes. 25 mg OD-Cu NPs were dispersed in 15 mL isopropanol and 75 μL Nafion (5 wt%) and sonicated for 1 hour. The suspension was then sprayed onto carbon paper (Sigracet 39BB) at 85°C with a spray-coater to achieve an active particle loading of ~1 mg/cm^2.

Sputtered Cu

100 nm of Cu was sputtered on carbon fiber paper using an AJA Magnetron Sputter System with a high purity Cu target. The Cu was sputtered in 3 mTorr Ar at 100 W, corresponding to a measured deposition rate of 1 Å/s. The stage was rotated at 100 rpm during the deposition.

Setup of GDE Cell

The setup of the GDE flow cell is described in detail in the Supplementary Information of ref. [30].

In brief, a custom-built gas tight PEEK cell was used for the electrochemical CO or CO_2 reduction, with a geometric area of 1 cm^2 for the working electrode. The cell consisted of anodic and cathodic compartments, which were separated by an anion-exchange membrane (Selemion). Each compartment was filled with 5 ml of aqueous 1 M KOH (99.99%, Sigma-Aldrich). The electrolytes were cycled through the system with a peristaltic pump (MasterFlex, Cole-Palmer) at 1 ml/min.

The potentials reported in this work are all referenced against the RHE:

$$E\ (\text{vs. RHE}) = E\ (\text{vs. Ag/AgCl}) + 0.197\ \text{V} + (\text{pH} \times 0.059\ \text{V}).$$

A platinum foil was used as counter electrode and an Ag/AgCl (saturated 3 M KCl) was used as reference electrode. The electrochemical measurements were performed with a BioLogic SP-300 potentiostat.

Real-Time Mass Analyzer Mass Spectrometer (RTGA-MS)

Mass spectra were collected using a Diablo 5000A Real-Time Gas Analyzer (RTGA) from Diablo Analytical, Inc.[59] The instrument is able to monitor gaseous input streams. The hardware consists of an Agilent Technologies 5975C high-performance quadrupole mass spectrometer, with the Real-Time Gas Analyzer hardware interface: a vacuum isolation valve, associated plumbing, and an MKS PDR2000 controller with a high-performance capacitance manometer pressure gauge. The vacuum in RTGA component is maintained by an Edwards nXDS-10i dry scroll pump (nominal pumping speed: 11.4 m^3/h), while the vacuum in the MSD is maintained by a Pfeiffer turbo pump with an Edwards RV12 (nominal pumping speed: 12 m^3/h) backing pump. The analyzer is controlled by the Agilent MSD ChemStation software. Method file creation and data processing are done by the Diablo MS Sensor 3.0 software.

This system provides chemical quantitation and speciation with wide dynamic range (10^4) in near real time. It provides a level of mass axis stability, dynamic range, speed of response, and calibration ease that is not possible with residual gas analyzers (RGAs). Although electron ionization (EI) was used, the background count was still within satisfactory range. For example,

pure ^{12}CO gas into the RTGA-MS, yielded ~200000 signal counts for *m/z* 28. The S/N at *m/z* 28 was about ~80, so the signal is still in large excess in comparison with the noise. The isotopic mass ^{13}CO at *m/z* 29 also gave about background S/N ~30.

A two-stage differential pumping scheme needed to get from 1 atm down to 10^{-6} Torr is used, which involves a sampling interface consisting of a sampling tee and a sampling cross (**Supplementary Fig. 2**).[59] Sample input tubing is connected to the top of the sampling tee. Any excess sample is then vented through the bottom branch of the tee. Only a small limited fraction of sample input flow is drawn through the sample orifice (30 μm i.d.) into the sampling cross. The bottom of the sampling cross is attached to a large bypass vacuum pump which pulls the majority of the sampled stream out as waste while reducing the pressure in the cross (monitored by a manometer). A second orifice (high vacuum orifice, 50 μm i.d.) further limits the amount of sample reaching the mass spectrometer and maintains the necessary high vacuum (typically 1×10^{-6} Torr), bearing some similarity to skimmers used in molecular beams. Finally, the mass spectrometer is separated from the sampling cross by an isolation valve. The gas stream can be introduced to the ionization region by opening the valve.

Modification of MS for Real-Time Detection

To enable real-time detection of electrochemical CO or CO_2R in GDE cells, the sampling tee was modified to enable few second time response, even at ultra-low flow rates (≤ 5 sccm), which is a critical step in order to measure the typical outputs from small electrochemical cells. We rigorously limited the dead volume in the sampling scheme to drastically improve time response. With this setup, the response time measured for a CO_2 gas tank (99% purity) was measured to display a fast response within 1–3 seconds, as shown in **Supplementary Fig. 3**.

Integration of the Modified RTGA-MS Setup with the GDE Cell

The experimental setup that is able to accomplish quick time response of electrochemical gas products is displayed in **Supplementary Fig. 1**.

A 1 m long tube (ETFE Plastic Semi-Clear Tubing, 1/8" OD and 1/16" ID) was used to attach the output gas stream from the gas diffusion electrode (GDE) cell to the inlet of the mass spectrometer.

The following calculation was performed to account for possibility of interdiffusion within the tube:

Inner diameter of tube = 1/16" = 1.57 mm = 0.157 cm

Inner radius of tube, r = 0.0785 cm

Area of cross-section of tube = πr^2 = 0.0194 cm^2

Flow rate = 5 sccm = 5 cm^3/min

Time delay between voltage applied to appearance of MS signal = 26 seconds

Vol. of gas in a 26 second pulse = 2.167 cm^3

Travel distance of gas from GDE to the 1st orifice = 2.167 cm^3/0.0194 cm^2 = 1.12 m

As the calculated travel distance matches the length of tube that was used (with some small tube connectors), there is no interdiffusion.

To control the inlet flow of gas into the GDE, a mass flow controller (MFC, Alicat Scientific) with a 0.5–100 sccm range was used. For the isotope labeled gas switching experiment, two of these MFCs and a VICI Valco Cheminert C25Z-3186UMH 4 port valve were employed.

A 10 ft long plastic tube (Abrasion-Resistant ETFE Plastic Semi-Clear Tubing for Chemicals, 1/64" ID, 1/16" OD, 10 Feet Long, McMaster-Carr), and attached to the outlet port of the sampling tee to prevent back-diffusion of air into the sampling tee. In addition, a steel Swagelok cap was lightly hand-tightened on the end to further limit back-diffusion of air.

The MS source temperature was set to 230°C, and the MS quadrupole set to 150°C.

UV-Vis Spectroscopy of Electrolyte

A Cary 60 UV-Vis spectrometer from Agilent Technologies was employed in the dual beam mode (scan speed: 600 nm/min) to collect the absorbance spectra for spectral determination of dissolved Cu species. To a plastic 3.5 ml cuvette, 850 µl of dmphen (2,9-dimethyl-1,10-phenanthroline) dissolved in ethanol (10 mM) was added to 3 ml of electrolyte (1 M KOH). A faint yellow tint was noted after the addition of dmphen to the used electrolyte.

Data availability

The data that supports the findings of this study are available upon reasonable request.

Acknowledgements

The authors would like to thank Heinz Frei for valuable insights regarding the status of current mass spectrometric methods, Frances A. Houle, Peter Agbo and Philipp S. Simon for helpful discussions, and gratefully acknowledge Adam Z. Weber and Xiong Peng for providing access to the RTGA-MS instrument. This work was supported by the Clean Energy Manufacturing Program, U.S. Department of Energy, Office of Science, Office of Basic Energy Sciences, Chemical Sciences, Geosciences, and Biosciences Division, under contract no. DE-AC02-05CH11231. Y.K. acknowledges fellowship support from the KAIST-UC Berkeley-VNU Climate Change Research Center (grant no. 2021K1A4A8A01079356).

Author contributions

H.J.Z. conceptualized the study, designed and renovated the mass spectrometer for fast time response at ultra-low flow rates, developed the methodology, performed experiments, analyzed and validated data, wrote the original draft of manuscript and revised the manuscript. Y.K. performed experiments and reviewed the manuscript. J.Y. acquired funding, administered the project, supervised the project and reviewed and edited the manuscript. J.W.A. conceptualized the

study, developed the methodology, acquired funding, administered the project, supervised the project and reviewed and edited the manuscript.

Ethics declarations

The authors declare no competing interests.

References

1. Tang, C., Zheng, Y., Jaroniec, M. & Qiao, S.-Z. Electrocatalytic refinery for sustainable production of fuels and chemicals. *Angew. Chem. Int. Ed.* **60**, 19572–19590 (2021).

2. Vogt, E. T. C. & Weckhuysen, B. M. The refinery of the future. *Nature* **629**, 295–306 (2024).

3. Bushuyev, O. S. *et al.* What should we make with CO_2 and how can we make it? *Joule* **2**, 825–832 (2018).

4. Huang, Z., Grim, R. G., Schaidle, J. A. & Tao, L. The economic outlook for converting CO_2 and electrons to molecules. *Energy Environ. Sci.* **14**, 3664–3678 (2021).

5. Zhu, P. & Wang, H. High-purity and high-concentration liquid fuels through CO_2 electroreduction. *Nat. Catal.* **4**, 943–951 (2021).

6. Shin, H., Hansen, K. U. & Jiao, F. Techno-economic assessment of low-temperature carbon dioxide electrolysis. *Nat. Sustain.* **4**, 911–919 (2021).

7. Hori, Y. Electrochemical CO_2 reduction on metal electrodes. in *Modern Aspects of Electrochemistry* (eds Vayenas, C. G., White, R. E. & Gamboa-Aldeco, M. E.) 89–189 (Springer New York, New York, NY, 2008). doi:10.1007/978-0-387-49489-0_3.

8. Nitopi, S. *et al.* Progress and perspectives of electrochemical CO_2 reduction on copper in aqueous electrolyte. *Chem. Rev.* **119**, 7610–7672 (2019).

9. Pander III, J. E., Ren, D. & Yeo, B. S. Practices for the collection and reporting of electrocatalytic performance and mechanistic information for the CO_2 reduction reaction. *Catal. Sci. Technol.* **7**, 5820–5832 (2017).

10. Burdyny, T. & Smith, W. A. CO_2 reduction on gas-diffusion electrodes and why catalytic performance must be assessed at commercially-relevant conditions. *Energy Environ. Sci.* **12**, 1442–1453 (2019).

11. Seger, B., Robert, M. & Jiao, F. Best practices for electrochemical reduction of carbon dioxide. *Nat. Sustain.* **6**, 236–238 (2023).

12. Vavra, J. *et al.* Solution-based Cu^+ transient species mediate the reconstruction of copper electrocatalysts for CO_2 reduction. *Nat. Catal.* **7**, 89–97 (2024).

13. Kim, I. *et al.* Unveiling the reconstruction of copper bimetallic catalysts during CO_2 electroreduction. *Nat. Catal.* **8**, 697–713 (2025).

14. Yang, Y. *et al.* Operando probing dynamic migration of copper carbonyl during electrocatalytic CO_2 reduction. *Nat. Catal.* **8**, 579–594 (2025).

15. Shannon, S. L. & Goodwin, J. G. Jr. Characterization of catalytic surfaces by isotopic-transient kinetics during steady-state reaction. *Chem. Rev.* **95**, 677–695 (1995).

16. van Dijk, H. A. J., Hoebink, J. H. B. J. & Schouten, J. C. Steady-state isotopic transient kinetic analysis of the Fischer–Tropsch synthesis reaction over cobalt-based catalysts. *16th Int. Conf. Chem. React. Eng.* **56**, 1211–1219 (2001).

17. Pérez-Ramírez, J. & Kondratenko, E. V. Evolution, achievements, and perspectives of the TAP technique. *Catal. Today* **121**, 160–169 (2007).

18. Berger, R. J. *et al.* Dynamic methods for catalytic kinetics. *Appl. Catal. Gen.* **342**, 3–28 (2008).

19. Athariboroujeny, M. *et al.* Competing mechanisms in CO hydrogenation over Co-MnO_x catalysts. *ACS Catal.* **9**, 5603–5612 (2019).

20. Raub, A., Karroum, H., Athariboroujeny, M. & Kruse, N. Chemical transient kinetics in studies of the Fischer–Tropsch reaction and beyond. *Catal. Lett.* **151**, 613–626 (2021).

21. Yang, Q. *et al.* Understanding of the fate of α-Fe_2O_3 in CO_2 hydrogenation through combined time-resolved *in situ* characterization and microkinetic analysis. *ACS Catal.* **13**, 9064–9077 (2023).

22. Wolter, O. & Heitbaum, J. Differential electrochemical mass spectrometry (DEMS) — A new method for the study of electrode processes. *Berichte Bunsenges. Für Phys. Chem.* **88**, 2–6 (1984).

23. Clark, E. L., Singh, M. R., Kwon, Y. & Bell, A. T. A novel differential electrochemical mass spectrometer cell design for online quantification of the products produced during electrochemical reduction of CO_2. *Anal. Chem.* **87**, 8013–8020 (2015).

24. Clark, E. L. & Bell, A. T. Differential electrochemical mass spectrometry (DEMS) cell. https://patents.google.com/patent/US10777396B2/en (2020).

25. Bondue, C. J. & Koper, M. T. M. A DEMS approach for the direct detection of CO formed during electrochemical CO_2 reduction. *J. Electroanal. Chem.* **875**, 113842–113842 (2020).

26. Baltruschat, H. Differential electrochemical mass spectrometry. *J. Am. Soc. Mass Spectrom.* **15**, 1693–1706 (2004).

27. Khanipour, P. *et al.* Electrochemical real-time mass spectrometry (EC-RTMS): Monitoring electrochemical reaction products in real time. *Angew. Chem. Int. Ed.* **58**, 7273–7277 (2019).

28. Vandergrift, G. W., Krogh, E. T. & Gill, C. G. Polymer inclusion membranes with condensed phase membrane introduction mass spectrometry (CP-MIMS): Improved analytical response time and sensitivity. *Anal. Chem.* **89**, 5629–5636 (2017).

29. Allard, S. & Lauritsen, F. R. Membrane inlet mass spectrometry (MIMS) for analysis of water disinfection byproducts: Recent advances. *TrAC Trends Anal. Chem.* **165**, 117141 (2023).

30. Kim, C. *et al.* Importance of site diversity and connectivity in electrochemical CO reduction on Cu. *ACS Catal.* **14**, 3128–3138 (2024).

31. Ren, H. *et al.* Operando proton-transfer-reaction time-of-flight mass spectrometry of carbon dioxide reduction electrocatalysis. *Nat. Catal.* **5**, 1169–1179 (2022).

32. Li, C. W., Ciston, J. & Kanan, M. W. Electroreduction of carbon monoxide to liquid fuel on oxide-derived nanocrystalline copper. *Nature* **508**, 504–507 (2014).

33. Verdaguer-Casadevall, A. *et al.* Probing the active surface sites for CO reduction on oxide-derived copper electrocatalysts. *J. Am. Chem. Soc.* **137**, 9808–9811 (2015).

34. Lobaccaro, P. *et al.* Initial application of selected-ion flow-tube mass spectrometry to real-time product detection in electrochemical CO_2 reduction. *Energy Technol.* **6**, 110–121 (2018).

35. Mandal, L. *et al.* Investigating the role of copper oxide in electrochemical CO_2 reduction in real time. *ACS Appl. Mater. Interfaces* **10**, 8574–8584 (2018).

36. Prajapati, A. *et al.* Best practices for in-situ and operando techniques within electrocatalytic systems. *Nat. Commun.* **16**, 2593–2593 (2025).

37. Arán-Ais, R. M., Scholten, F., Kunze, S., Rizo, R. & Roldan Cuenya, B. The role of in situ generated morphological motifs and Cu(I) species in C_{2+} product selectivity during CO_2 pulsed electroreduction. *Nat. Energy* **5**, 317–325 (2020).

38. Timoshenko, J. *et al.* Steering the structure and selectivity of CO_2 electroreduction catalysts by potential pulses. *Nat. Catal.* **5**, 259–267 (2022).

39. Kok, J., Albertini, P. P., Leemans, J., Buonsanti, R. & Burdyny, T. Overcoming copper stability challenges in CO_2 electrolysis. *Nat. Rev. Mater.* **10**, 550–563 (2025).

40. Vavra, J., Shen, T.-H., Stoian, D., Tileli, V. & Buonsanti, R. Real-time monitoring reveals dissolution/redeposition mechanism in copper nanocatalysts during the initial stages of the CO_2 reduction reaction. *Angew. Chem. Int. Ed.* **60**, 1347–1354 (2021).

41. Popovic, S., Bele, M. & Hodnik, N. Reconstruction of copper nanoparticles at electrochemical CO_2 reduction reaction conditions occurs via two-step dissolution/redeposition mechanism. *ChemElectroChem* **8**, 2634–2639 (2021).

42. Kim, H. *et al.* Dynamic interface engineering via mechanistic understanding of copper reconstruction in electrochemical CO_2 reduction reaction. *J. Am. Chem. Soc.* **148**, 6045–6056 (2026).

43. Hori, Y. *et al.* "Deactivation of copper electrode" in electrochemical reduction of CO_2. *Electrochimica Acta* **50**, 5354–5369 (2005).

44. Serra-Maia, R. *et al.* Decoupling CO_2 effects from electrochemistry: A mechanistic study of copper catalyst degradation. *iScience* **28**, 111851 (2025).

45. Lee, S. H. *et al.* Structural transformation and degradation of Cu oxide nanocatalysts during electrochemical CO_2 reduction. *J. Am. Chem. Soc.* **147**, 6536–6548 (2025).

46. Lum, Y. & Ager, J. W. Two active sites are better than one. *Nat. Catal.* **6**, 864–865 (2023).

47. Tang, W. *et al.* The importance of surface morphology in controlling the selectivity of polycrystalline copper for CO_2 electroreduction. *Phys. Chem. Chem. Phys.* **14**, 76–81 (2012).

48. Liu, X. *et al.* Understanding trends in electrochemical carbon dioxide reduction rates. *Nat. Commun.* **8**, 15438 (2017).

49. Zhang, J. *et al.* Isotopic labelling of water reveals the hydrogen transfer route in electrochemical CO_2 reduction. *Nat. Chem.* **17**, 334–343 (2025).

50. Lum, Y. & Ager, J. W. Evidence for product-specific active sites on oxide-derived Cu catalysts for electrochemical CO_2 reduction. *Nat. Catal.* **2**, 86–93 (2019).

51. Gao, W., Xu, Y., Fu, L., Chang, X. & Xu, B. Experimental evidence of distinct sites for CO_2-to-CO and CO conversion on Cu in the electrochemical CO_2 reduction reaction. *Nat. Catal.* **6**, 885–894 (2023).

52. Hagman, B. *et al.* Steps control the dissociation of CO_2 on Cu(100). *J. Am. Chem. Soc.* **140**, 12974–12979 (2018).

53. Wang, X. *et al.* Mechanistic reaction pathways of enhanced ethylene yields during electroreduction of CO_2–CO co-feeds on Cu and Cu-tandem electrocatalysts. *Nat. Nanotechnol.* **14**, 1063–1070 (2019).

54. Li, Y. & Yang, P. Co-feeding copper catalysts couple carbon. *Nat. Nanotechnol.* **14**, 1002–1003 (2019).

55. Lin, W.-Y. *et al.* Identification of CO_2 as a reactive reagent for C–C bond formation via copper-catalyzed electrochemical reduction. *ACS Catal.* **13**, 11697–11710 (2023).

56. Zhang, Q. *et al.* Atomic dynamics of electrified solid–liquid interfaces in liquid-cell TEM. *Nature* **630**, 643–647 (2024).

57. Mayer, J. M. Site heterogeneity and broad surface-binding isotherms in modern catalysis: Building intuition beyond the Sabatier principle. *J. Catal.* **439**, 115725–115725 (2024).

58. Kim, S. *et al.* A new era in operando. *Nat. Catal.* **9**, 245–247 (2026).

59. Terry Ramus. Diablo 5000A RTGA Getting Started Manual by Diablo Analytical, Inc. *https://diabloanalytical.com/rtga/files/5000A%20Getting%20Started%20Manual.pdf* https://diabloanalytical.com/rtga/files/5000A%20Getting%20Started%20Manual.pdf (2014).